Mechanisms of Fouling, Slagging and Corrosion by Pulverized Coal Combustion

M.E. Gulden, L.L. Hsu and A.R. Stetson

July 1981

Quarterly Technical Progress Report No. 1
Contracting Period: March 11, 1981 to June 11, 1983
Reporting Period: March 11 to June 30, 1981

Contract DE-AC22-81PC-40272

Prepared for

Pittsburgh Energy Technology Center
U.S. Department of Energy
P.O. Box 10940
Pittsburgh, Pennsylvania 15236

SR81-R-4930-05

SOLAR TURBINES INTERNATIONAL
2200 Pacific Highway, P.O. Box 80966, San Diego, California 92138

DISCLAIMER

Mechanisms of Fouling, Slagging and Corrosion by Pulverized Coal Combustion

M.E. Gulden, L.L. Hsu and A.R. Stetson

July 1981

Quarterly Technical Progress Report No. 1
Contracting Period: March 11, 1981 to June 11, 1983
Reporting Period: March 11 to June 30, 1981

Contract DE-AC22-81PC-40272

Prepared for

Pittsburgh Energy Technology Center
U.S. Department of Energy
P.O. Box 10940
Pittsburgh, Pennsylvania 15236

SR81-R-4930-05

SOLAR TURBINES INTERNATIONAL
2200 Pacific Highway, P.O. Box 80966, San Diego, California 92138

THIS PAGE

WAS INTENTIONALLY

LEFT BLANK

ABSTRACT

This is the first quarterly progress report on Contract DE-AC22-81PC-40272.

The objective of this program is to conduct a detailed and comprehensive study of the mechanisms of fouling, slagging and corrosion in pulverized coal combustors by employing well controlled model systems which simulate the coal combustion environment.

Emphasis during this period has been on design and construction of the combustion test rig. All design phases are complete. Construction of the diffuser and test sections is also complete.

THIS PAGE

WAS INTENTIONALLY

LEFT BLANK

TABLE OF CONTENTS

TABLE OF CONTS (cont)

LIST OF FIGURES

THIS PAGE

WAS INTENTIONALLY

LEFT BLANK

LIST OF TABLES

1

INTRODUCTION

This is the first quarterly technical progress report on Contract DE-AC22-81PC-40272. The overall objective of this program is to conduct a detailed and comprehensive study of the mechanisms of fouling, slagging and corrosion in pulverized coal combustors by employing well controlled model systems which simulate the coal combustion environment.

Replacement of oil and natural gas by coal in industry is dependent upon solutions to several technical problems. Fouling, slagging and corrosion problems caused primarily by the mineral matter in the coal and its behavior subsequent to the combustion process is one of these problems. In the absence of adequate understanding of the physical and chemical events governing these problems, application to industrial boilers will be held back, and application to more advanced systems such as indirect or direct fired gas turbines cannot be considered.

The background and plan for this program is presented in the next section which is followed by sections on current results and future work.

THIS PAGE

WAS INTENTIONALLY

LEFT BLANK

2

BACKGROUND AND PROGRAM PLAN

A large number of observed or potential fouling, slagging and corrosion mechanisms will be tested in model systems designed to minimize side reactions. The fouling slagging mechanisms to be investigated are shown in Table 1; the corrosion mechanisms in Table 2. These mechanisms are based on published information on coal fouling, studies with other fuels, prior work at Solar, and theoretical concepts.

The simulated combustion tests will be conducted in a small gas fired combustor equipped with tubes at various temperatures and distances downstream to simulate boiler and heat exchanger heat transfer surfaces. Short term (approx. 1-50 hr) tests will be carried out in the combustor by adding various solid and vapor phase contaminants to the combustion products. As necessary, some of the tube specimens will be placed in a furnace with a slow-flowing controlled atmosphere for periods up to 100 hours to evaluate longer term effects. After the initial tests are performed, the resulting data will be analyzed and control techniques proposed. These control techniques will then be tested to evaluate their potential for reducing or eliminating fouling and corrosion problems.

For convenience, the program has been separated into the following tasks:

- Task I - Construction and Calibration of Test Rigs to Establish Correlation with Pulverized Coal Combustor
  - Task Ia - Design of Test Rigs
  - Task Ib - Construction of Test Rigs
  - Task Ic - Calibration of Test Rigs
- Task II - Parametric Study to Identify Rate Controlling Mechanisms for Fouling, Slagging and Corrosion
  - Task IIa - Defined Parametric Tests
  - Task IIb - Additional Tests
- Task III - Evaluation of Control Techniques
- Task IV - Analysis of Results

The program schedule is shown in Figure 1.

Table 1

Potential Fouling and Slagging Mechanisms

Mechanism	Schematic	Descripton With Example
F1. Condensate on Ash	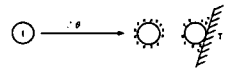	Vapor species (X) condenses on inert (non-reactive) ash particle (I) on cooling $\Delta\theta$. Liquid-coated particle sticks to cool target (T). Example: I = Al_2O_3 X = Na_2SO_4
F2. Ash Surface Reaction	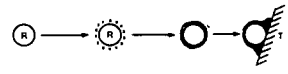	Condensate (X) on surface reacts with reactive ash particle (R) to form plastic product. Example: R = $Al_2O_3.6SiO_2$ X = NaCl $2NaCl + H_2O + Al_2O_3.6SiO_2 \rightarrow Na_2O.Al_2O_3.6SiO_2 + 2NaCl$
F3. Ash Plastic Flow	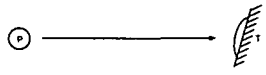	Plastic particle deforms to conform with surface and be mechanically attached (may react later). Well established for glass-behaving ash with viscosities between 10^4 and 250 poise.
F4. Adiabatic Plastic Flow of Ash	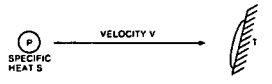	Temperature rise on deformation given by $\Delta\theta = V^2/sJ$. This is important for high velocities and high angle impacts. Example is $CaSO_4$ at 1000-1500°F. Deposition boundary moves to lower temperatures at high velocities and higher temperatures at low incident angles.
F5. Cementation on Surface	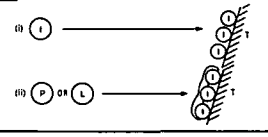	Step (i): non-sticking particles (I or R) impact surface followed quickly by Step (ii): plastic (P) or liquid (L) particles to cement mass together. Cementation also occurs by condensation of vapor species, especially alkali sulphate that may result
F6. Surface Condensation	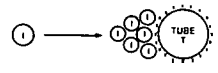	Vapor species (X) condenses on surface to provide sticky surface for entrapment and cementing of non-sticking particles (I or R). Observed for boiler tubes where X = Na_2SO_4 and build-up occurs only for high angle impacts (scale distorted for tube and particles)
F7. Sintering on Surface	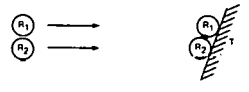	Sintering between similar particles ($R_1 = R_2$) or dissimilar particles ($R_1 \neq R_2$) to increase strength of deposit. Increases adherence by increasing resistance to thermal shock and erosion. Sintering may include target (or tube) T. Very sensitive to alkali content. Independent of the ash fusion and softening temperatures measured on gross sample.
F8. Reaction With Target (Tube)		Target (T) reacts with impacted particle R to increase strength of bond. Examples: metal tube where R = SiO_2: $Fe_2O_3 + SiO_2 \rightarrow Fe_2O_3.SiO_2$; ceramic tube where I = SiO_2 on surface and R = $CaSO_4$: $CaSO_4 + SiO_2 \rightarrow CaO.SiO_2 + SO_3$.
F9. Incomplete Ash Reaction (short residence time)		Inadequate residence time in combustor to complete reaction raises stickiness. Example: incomplete homogenization of silicate glasses leaving low viscosity, sticky regions; also incompletely burnt coal particles with surface tars.
F10. Reducing Reactions	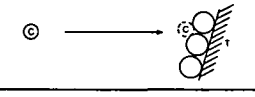	Reduction by carbon particles will lower viscosity if iron or other reducible oxide is present. Typical reduction of fouling temperature is 200°F.
F11. Deposition/ Erosion	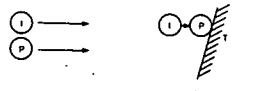	Mildly fouled surface by glassy siliceous particles (P) of high viscosity (e.g., 10^4 poise) may be eroded by semi-inert particles (I) of high abrasiveness such as mullite or quartz.
F12. Temperature Gradients	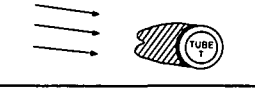	Temperature at surface of deposit increases to near gas temperature as build-up occurs. For constant wall temperature, surface sintering increases with gas temperature.

Table 2

Accelerated Corrosion Mechanisms

Mechanism	Schematic	Descripton With Example
1. Basic Fluxing or Oxide Ion Attack	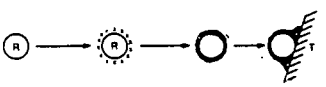	Impact or condensation of low melting phases, e.g., $MgSO_4 + Na_2SO_4$ eutectic is 1240°F; $NaCl + Na_2SO_4$ eutectic is 1150°F. Reaction is then followed by: $\cdot\ Na_2SO_4 + 4M \rightarrow 3MO + MS + Na_2O$ $- Na_2O + Al_2O_3 \rightarrow 2NaAlO_2$ $- 2Na_2O + Cr_2O_3 + 3/2\ O_2 \rightarrow 2Na_2CrO_4$ to yield a nonprotective oxide.
2. Acid Fluxing	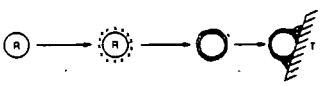	Impact or condensation of low melting eutectic e.g., Na_2O–V_2O_5 eutectic in this system is 986°F. Oxide ion content is lowered to a level that requires dissociation of protective oxides $Al_2O_3 \rightarrow 2Al^{3+} + 3O^{=}$ $Cr_2O_3 \rightarrow 2Cr^{3+} + 3O^{=}$ Dissolution of protective oxides results and linear oxidation ensues.
3. Liquid Phase Rapid Oxygen Transport	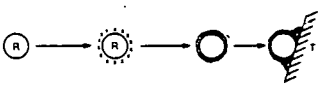	Deposition of multiple valence cation in low melting salt, e.g., $K_3Fe(SO_4)_3$. (Requires presence of SO_2). Rapid transport oxygen is possible by ion diffusion and convection. Air Interface: $4Fe^{2+} + O_2 \rightarrow 4Fe^{3+} + 2O^{=}$ Alloy Interface: $Fe^{3+} + Fe \rightarrow 2Fe^{=}$. The result is rapid oxidation and dissolution of iron salts or formation of iron and non-protective solid phase.
4. Solid Phase High Rate Oxygen Transport	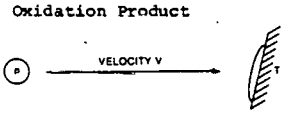	Same as #3 but does not require liquid present. All attack is by solid-state diffusion and consequently is a slower rate process than #3 but one that can produce thicker growths of oxide over long periods of time. Oxidation of low alloy steel above 850°F without any deposit is an example of this type of mechanism. Deposition of Fe_2O_3 produces this effect on higher temperature alloys at temperatures above 1400°F.

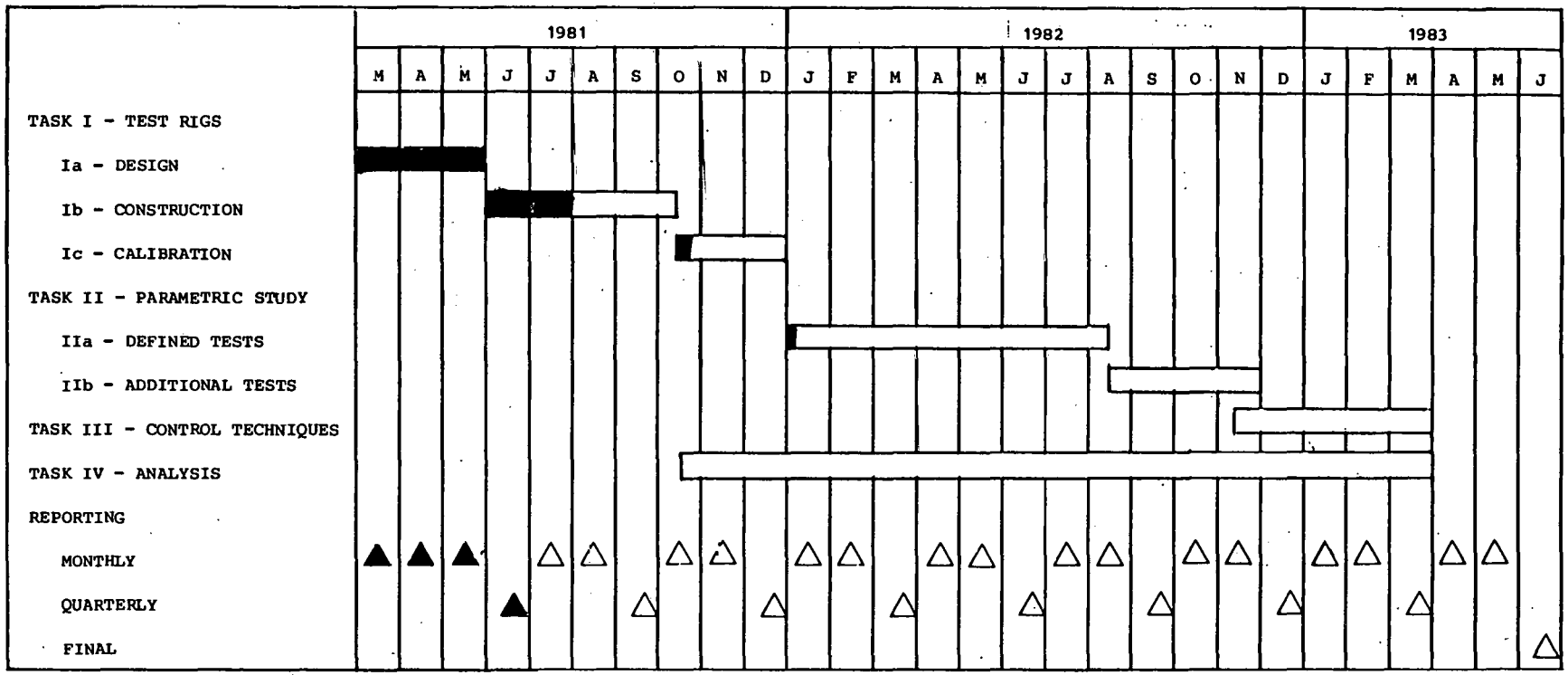

Figure 1. Program Schedule

Each task will be discussed separately.

2.1 TASK I - DESIGN, CONSTRUCTION, AND CALIBRATION OF TEST RIGS

This task will consist of three subtasks to design, construct and calibrate the test rigs that will be used in subsequent tasks for elucidating and understanding the mechanisms of fouling, slagging and corrosion associated with pulverized coal combustion.

2.1.1 Task Ia - Design of Test Rigs

Combustion Rig

The existing environmental simulator burner rig facilities will be redesigned for this program. The reversed flow can-type combustor design will be essentially retained with the necessary modification for introduction of salt solution and powder particles through the fuel nozzle. The combustor will be designed for operation with natural gas at atmospheric pressure. Aerodynamic and thermal analyses will be performed to achieve the following primary goals:

1. Efficient mixing of the particles in the gas stream.
2. Good atomization of salt solution to obtain uniform distribution of salt in the gas stream.
3. Gas stream approach velocity of 50 ft/sec and 2300°F temperature at first target bank.
4. Particle velocity approaching gas velocity.
5. Sufficient residence time for equilibrium of particle temperature with gas temperature.

In addition to the above, the rig design will also include access for sampling and for making measurements such as particle velocity, temperature, distribution, and gas velocity, temperature and composition. At the exhaust end of the combustion rig, a particle separator or ash collector will allow sampling of incinerated ash and also will remove exhaust particulates in compliance with local environmental regulations.

Furnace Rig

The furnace rig will be used primarily to study corrosion phenomenon associated with fouled tubes. The gaseous constituents typical of the combustor rig will be obtained by selective addition of various gases. Total mass flow rates will be kept low and all incoming gases will be brought to temperature in a preheater.

2.1.2 Task Ib - Construction of Test Rigs

Both combustor and furnace rigs will be constructed as designed, including systems such as exhaust ducting, particle loader, and control instrumentation.

2.1.3 Task Ic - Calibration of Test Rigs - Combustion Rig

The combustion rig will be fully characterized in order to have well described baseline test conditions. Characterization and analysis will include the following.

Velocity

Gas velocities will be measured at several locations and before each bank of specimens. This will allow dimensional mapping of the gas stream velocities. Particle velocity will be determined at the first and second bank locations and corresponding calculations will be performed to compare results.

Temperature

Gas, particle, and target tube temperatures will be determined experimentally. Gas stream temperature will be used in the control feedback loop to monitor fuel levels. Particle temperature will be measured using either two-color or disappearing-filament pyrometry. Target temperatures at the leading edge of the tubes will be monitored by thermocouples imbedded in the substrate.

Gas Stream Composition and Distribution

Suspension of particulates in the gas stream will be carefully monitored to ensure uniform cross sectional flow at the target banks. Chemical composition of the gas stream will be analyzed to determine the concentration levels of CO_2, O_2, N_2, SOx, NOx, hydrocarbon and salt additions. Gas sampling ports will be located before and after each target bank and sampling frequency will depend on the requirements of each test and the phenomenon under study.

Furnace Rig. Calibration of tests for the furnace rig will consist of demonstrating good control over the chemical composition and mixing of the various gaseous constituents simulating combustion effluent. Temperature and mass flow will be determined for each test and continuous monitoring will be utilized for long term exposures.

2.2 TASK II - PARAMETRIC STUDY TO IDENTIFY RATE CONTROLLING MECHANISMS FOR FOULING, SLAGGING AND CORROSION

Approximately 34 test groups will be evaluated to determine controlling mechanisms (see Tables 1 and 2) for specific species and combination of species which are common products of pulverized coal (PC) combustion. As many as five tests will be performed in each test group to determine significant levels of contamination, rates of reaction, and verification of mechanisms. The main parameters to be investigated are:

- Non-condensing alkali (NaCl)
- Condensing alkali (Na_2SO_4, K_2SO_4)
- Alkali ratio (Na/K) - melting point depression
- Inert particles (Al_2O_3)
- Reactive particles ($SiO_2.Fe_2O_3$)
- Ash viscosity (SiO_2, $Al_2O_3.CaO.Fe_2O_3$ glasses)
- Sulfur (SOx gas, $SO_4^=$)
- Incomplete combustion - reducing agent (carbon)
- Reactive surface area (SiO_2 particle size > standard SiO_2 particle size)
- Gas stream and particle velocity
- Tube material and temperature

Two sets of experiments will be performed. The first set consisting of test groups 1 through 25, as described in Task IIa, are well defined. The second set of approximately nine test groups, described in Task IIb, are not defined initially but will be formulated based on the results of Task IIa.

The test groups are designed to start with a simple system to isolate effects due to a single specie and progress up to an environment which simulates PC combustion products. The test groups, expected combustion gas interaction and potential fouling, slagging and corrosion mechanisms, are given in Table 3.

Six tube materials characteristic of boilers and heat exchanger application and operating at appropriate temperatures for each material will be used as targets. Materials and operating temperatures are as follows:

Table 3

Test Groups Proposed for Study

Test Group	Test System Variables: Gas Phase	Test System Variables: Solid Phase	Test System Variables: Other	Combustion Gas Interactions	Fouling, Slagging or Corrosion Mechanisms
1	NaCl	Al_2O_3	S-free gas	Noncondensing alkali + inert particle	Surface condensation on boiler tubes
2	NaCl	SiO_2	S-free gas	Noncondensing alkali + reactive particle	Ash surface reaction to increase surface stickiness
3	NaCl	SiO_2	Std	Noncondensing alkali + reactive particle	Effect of chloride conversion to sulphate on fouling
4	Na_2SO_4(m)	Al_2O_3	Std	Condensing alkali + inert particle	Comparison with sodium chloride (test group 1)
5	Na_2SO_4(m)	SiO_2	Std	Condensing alkali + reactive particle	Ash surface reaction to increase surface stickiness
6	Na_2SO_4(l)	SiO_2	Std	Condensing alkali + reactive particle	Effect of alkali concentration on deposition temperature
7	Na_2SO_4(h)	SiO_2	Std	Condensing alkali + reactive particle	Effect of alkali concentration on deposition temperature
8	Na_2SO_4(m)	SiO_2(l)	Std	Condensing alkali + reactive particle	Less complete reaction with large silica grains
9	K_2SO_4(m)	SiO_2	Std	Condensing alkali + reactive particle	Effect of sulphate melting point
10	$(Na,K)_2SO_4$(m)	SiO_2	Std	Condensing alkali + reactive particle	Effect of sulphate melting point
11	K_2SO_4(m)	$Fe_2(SO_4)_3$	Std	Reactive species to form complex sulphates	Effect of complex trisulphate on fouling and 1000-1300°F corrosion
12	K_2SO_4(m)	Fe_3O_4	Std/H_2S	Reactive species to form complex sulphates	Effect of iron oxides on fouling and slagging
13	Na_2SO_4(m)	to be selected from 11 and 12		Reactive species to form complex sulphates	Comparison of sodium and potassium complexes
14		Glass 5	Std	None	Effect of viscosity (10^5 poise at 2300°F) of incinerated ash on fouling
15		Glass 3.5	Std	None	Effect of viscosity ($10^{3.5}$ poise at 2300°F) of incinerated ash on fouling
16		Glass 2.5	Std	None	Effect of viscosity ($10^{2.5}$ poise at 2300°F) of incinerated ash on fouling
17		Glass 5	C	Reduction of iron in glass 5	Effect on fouling of reduction of viscosity in situ
18	Na_2SO_4(h)	Glass 5	Std	Condensing alkali + reactive particles	Cementation by sodium sulphate to increase fouling and sinter strength
19		Glass 4	V=20 fps	None	Effect of adiabatic plastic deformation on fouling by a marginal fouling species (assumed to be 10^4 poise at 2300°F)
20		Glass 4	V=50 fps	None	
21		Glass 4	V=200 fps	None	

Table 3 (Cont)

Test Groups Proposed for Study

Test Group	Test System Variables: Gas Phase	Solid Phase	Other	Combustion Gas Interactions	Fouling, Slagging or Corrosion Mechanisms
22		-	C	Combustion	Baseline to determine erosion by carbon
23	Na_2SO_4	-	C	Combustion	Effect of surface reduction on loss of protective oxides and hot corrosion (sulphidation)
24	Na_2SO_4		$C+H_2S$	Combustion	Effect of higher SOx on corrosion
25	-	Glass 5	Fe_3O_4	None	Increased sintering due to different species
26					
27					
28					
29					
30					
31					
32					
33					
34					

Notes: Gas phase additions at level l will have dewpoint ~1000F
Gas phase additions at level m will have dewpoint ~1500F
Gas phase additions at level h will have dewpoint ~2200F

Tube Material	Temperature
Ceramic (NC-430 - siliconized SiC)	2000°F, 1600°F
Superalloy (Hastelloy X)	1600°F
Stainless Steel (AISI 310)	1300°F
Croloy Alloy (2-1/4 Cr, 1 Mo steel)	1100°F
Stainless Steel (304H)	1000°F
Carbon Steel (ASME Spec. SA-210)	800°F

2.2.1 Task IIa - Defined Parametric Tests

Test Groups 1 and 2. The effect of a non-condensing alkali (NaCl) in the presence of inert (Al_2O_3) and reactive (SiO_2) particles in sulfur-free combustion gas will be evaluated. Particle sizes will be approximately 10 microns and less for all test groups unless mentioned specifically. The particle size distributions will be analyzed. Results of test groups 1 and 2 will also act as a baseline for future tests.

Test Group 3. $SOx_{(g)}$ will be introduced at the standard level of 10-25 ppm in the presence of NaCl and SiO_2 (same levels as tests 1 and 2) to activate conversion of chloride to sulfate. This standard level of $SOx_{(g)}$ will be used in the remainder of the tests.

Test Groups 4 and 5. Moderate levels (dewpoint approx. 1500°F) of a condensing alkali (Na_2SO_4) in the presence of reactive (SiO_2) and inert (Al_2O_3) particles will be examined.

Test Groups 6 and 7. The effect of Na_2SO_4 concentration will be determined by a high level (dewpoint approx. 2200°F) and a low level (dewpoint approx. 1000°F) both in the presence of reactive particles (SiO_2).

Test Group 8. The contribution of total reactive surface area will be assessed through use of larger reactive particles (approx. 30 microns SiO_2) with a condensing alkali (Na_2SO_4).

Test Groups 9 and 10. The effect of melting point variation of alkali sulfates will be evaluated through introduction of K_2SO_4 (melting point 1960°F) and a 80 mole % Na_2SO_4.20 mole % K_2SO_4 mixture (melting point 1513°F) with SiO_2 particles.

Test Groups 11, 12 and 13. The contribution of complex iron trisulfates will be determined by testing with $K_2SO_4 + Fe_2(SO_4)_3$, $K_3SO_4 + Fe_3O_4$ plus additional $SOx_{(g)}$, and Na_2SO_4 with either $Fe_2(SO_4)_3$ or Fe_3O_4 plus additional $SOx_{(g)}$.

Test Groups 14, 15 and 16. Viscosity of particles will be investigated through use of three glass compositions with viscosities of approximately 10^5, $10^{3.5}$ and $10^{2.5}$ poise at 2300°F. The glasses will be smelted, fritted, milled and sized at Solar. The glasses will be based on the oxides SiO_2, Al_2O_3, CaO and Fe_3O_4. The particle sizes will be equivalent to the Al_2O_3 and SiO_2 particles used in earlier tests (approx. 10 microns and less). Particle size distributions will be measured as well as glass viscosity for each composition.

Test Group 17. The potential of a reducing agent (carbon particles) to lower viscosity will be evaluated with the high viscosity (10^5 poise) glass.

Test Group 18. The effect of a condensing alkali (Na_2SO_4) in the presence of a high viscosity glass will be evaluated.

Test Groups 19, 20 and 21. Effect of particle velocity on deposition will be assessed by using 10^4 poise glass particles at velocities of 20, 50 and 200 fps.

Test Groups 22, 23 and 24. Effect of reducing agent (carbon particles) on reactions will be evaluated. Specific test variables will depend on results from previous tests, but will probably include carbon alone, carbon plus Na_2SO_4, and carbon plus Na_2SO_4 plus $SOx_{(g)}$.

Test Group 25. Potential of Fe_3O_4 to reduce glass viscosity will be assessed using the high viscosity (approx. 10^5 poise) glass.

2.2.2 Task IIb - Additional Tests

Test Groups 26 through 34. Selection of specific variables in the remaining test groups will be based on results from the test groups discussed above, discussion with PETC engineering personnel, and continuing literature review. Particle size may be studied in greater depth. Also, it is expected that a complex system will be included, for example: $SiO_2.Al_2O_3.CaO.Fe_2O_3$ glass plus Fe_2O_3 plus Na_2SO_4 plus $SOx_{(g)}$, which closely simulates typical P.C. combustion products. Tests may also involve heavier particle loading than the standard loading rate of approximately 1 lb/hr or 1 lb/900 lbs of gas to more closely simulate the particulate concentrations after PC combustion. If considered important, aerodynamic effects will be considered by comparing axial flow with the standard cross flow gas path results.

The above test groups will all be performed in the combustion test rig described in Section 2.1. Some of the specimens will then be subjected to furnace rig tests to investigate long term corrosion and reaction effects. Specimens from test groups 23 and 24 are examples of likely candidates.

2.3 TASK III - CONTROL TECHNIQUES

Tests to evaluate control techniques will be conducted in this phase of the program. Selection of test variables will be based on the important fouling, slagging and corrosion mechanisms derived from Task II work. The combustion products may be synthesized (analogous to complex systems from Task II) and/or by ash collected from Solar's PC combustor. Potential additive materials based on current literature incude $CaCO_3$, dolomite and diatomaceous earth.

2.4 TASK IV - ANALYSIS OF RESULTS

The mechanism of fouling, slagging and corrosion for known operating conditions will be determined through characterization of the tube specimens and the gas phase, including particulates. The principal analytical technique for tube specimens will be scanning electron microscopy (SEM) used in conjunction with energy dispersive X-ray (EDX) analysis. As necessary, additional analytical techniques will be utilized to elucidate the controlling mechanisms. Examples of these techniques are X-ray fluorescence and diffraction, atomic absorption, electron microprobe analysis, and electron diffraction.

Particulates in the gas stream will also be characterized using the above techniques. The gas phase will be analyzed using standard emission monitoring methods for oxides of carbon, nitrogen, sulfur, and hydrocarbons, and standard chemical techniques for sulfur oxides and soluble constituents such as sulfates and chlorides. A listing of the chemical and diagnostic tests to identify the potential fouling, slagging and corrosion mechanisms is given in Table 4.

Table 4

Chemical and Diagnostic Tests

Test Group	Fouling, Slagging or Corrosion Mechanisms	Tests	Diagnostics
1-2	Sorption and reaction of NaCl with Al_2O_3 or SiO_2	Quantitative measurement of sorbed Na^+, Cl^- and soluble SiO_3 (AlO_2^-) by AA, specification electrode, X-ray fluorescence on particles and deposits	Ionic balances: $[Na+]=[Cl^-]+1/2[SiO_3^=]$ or $[AlO_2]^-$ If soluble $SiO_3^=$ present, X-ray diffraction of particles and deposits.
3	Conversion of NaCl to Na_2SO_4 by SO_x	SO_2 and SO_3 partial pressures by ASTM D2914. Quantitative measurement of soluble Na^+, Cl^-, $SO_4^=$, $SiO_3^=$ by AA, specific ion electrode, X-ray fluorescense on particles and deposits	Ionic balances: $[Na+]+(M+)=(Cl^-)+1/2(SO_4^=)+1/2(SiO_3^=)$ If soluble SiO_3 present, X-ray diffraction of particles and deposits.
4-5	Condensing alkali and inert reactive particles	SO_2 and SO_3 partial pressure by ASTM D2914. Quantitative measurements of soluble Na^+,, $SO_4^=$, $SiO_3^=$, AlO_2^- by AA, X-ray fluorescense on particles and deposits	Ionic balances If soluble $SiO_3^=$ or AlO_2^- then X-ray diffraction of particles and deposits. Compare results with test groups 1-3 to determine effect of condensing alkali.
6-7	Effect of alkali concentration on deposition temperature	Same as test groups 4-5	Same as test group 4-5. Compare data with above groups to determine effect of alkali concentration.
8	Effect of less complete reaction with large silica grain	Same as test groups 4-5	Same as test groups 4-7. Compare data with test group 7 to determine the effect of SiO_2 grain size.
9-10	Effect of sulfate melting point	SO_2 and SO_3 partial pressure by ASTM D2914. Quantitative measurement of soluble Na^+, K^+, $SO_3^=$, $SiO_3^=$ by AA, X-ray fluorescense on particle and deposits	Ionic balances. If soluble $SiO_3^=$ X-ray diffraction on particles and deposits. Compare data with test groups 4-8 to determine effect of $SO_4^=$ melting point on mechanisms
11-13	Effect of complex trisulfates on iron oxide as sodium or potassium on fouling/slagging and 1000-1300°F corrosion	SEM-EDAX and EMP composition of tube materials in contact with deposits	Depth of penetration and identification of corrosion products. Correlate with literature (Ref. 13).

Table 4 (Cont)

Chemical and Diagnostic Tests

Test Group	Fouling, Slagging or Corrosion Mechanisms	Tests	Diagnostics
14-16	Effect of ash viscosity on fouling	SEM-EDAX, X-ray fluorescent and AA of particles and deposits to determine composition change, if any. X-ray diffraction of particles and deposits to note changes in atomic structure.	None planned
17	Effect of lowering viscosity by reducing conditions in fouling	SEM-EDAX, X-ray fluorescent and AA of particles and deposits to determine composition change. Ferrous/ferric ratio by dissolution in HF and titration with $CrO_4^=$	Comparison of ferrous/ferric ratio change between formed, caught and deposited particles
18	Cementation by sodium sulphate on fouling and sintering strength	Same as test groups 14-16. No chemical tests are contemplated since mostly mechanical effects are to be investigated	None
19-21	Effect of adiabatic plastic deformation on fouling	Same as test group 18	None
22-24	Effect of unburnt coal on fouling, slagging and corrosion	SEM-EDAX, X-ray fluorescent, AA and X-ray diffraction analysis of paraticles and deposits. SEM-EDAX and EMP of substrates and deposits. Ferrous ferric ratio by HF dissolution of particles and deposits.	Compare composition and atomic structure changes as particles react, deposit and cause corrosion.
25	Effect of higher SOx on corrosion	SO_2 and SO_3 partial pressures by ASTM D2914. SEM-EDAX and EMP analysis of tubes in contact with deposits	Correlate with data from test groups 11-13 and other groups where corrosion noted, identify corrosion products.
26-34	To be planned during program	Same as test groups 1-25	

3

CURRENT RESULTS

Work during this first quarter has centered on Task Ia and Ib, design and construction of the test rigs and procurement of the materials required for execution of the program.

3.1 TASK Ia - DESIGN OF TEST RIGS

This phase of the program is complete.

A complete set of engineering drawings for the combustion rig is given in Appendix A. Figure 2 shows a schematic of the entire combustion test rig with principal features labeled.

The rig will be supported vertically with the combustor unit mounted at the top, followed by the diffuser section (18" long, 9° angle). The two 18-inch long test sections are identical units, measuring 4 by 10 inches internally. A slotted section is provided in each test section for location of a bank of six specimen tubes. These slots will also serve as access ports for measuring gas temperature and velocity as well as for particle sampling. Just upstream of the specimen bank is a pair of viewing ports which will also be used for particle temperature measurement. After leaving the second test section, combustion gases will enter the exhaust duct with two 90-degree bends to allow particles to settle out of the gas stream. Water spray will be employed to enhance particle agglomeration and removal. Any additional particle sampling required at this stage (e.g., incinerated ash) will be conducted via the sampling port upstream of the water spray.

The fuel injector for the combustor (Fig. A-2) was redesigned to allow injection of natural gas, salt solutions, and particulates. Particle distribution in the gas stream will be determined by using an isokinetic sampling probe specifically designed for this purpose (Fig. A-3). The annular design allows the probe to be water cooled with the solid particles flowing through the probe, at the same velocity as in the test section. The probe will be connected to a smoke monitor whereby the solids will be trapped on a pre-weighed filter paper with the aid of a mechanical pump.

A schematic of the furnace rig is shown in Figure 3. Instead of the double tube furnace system originally proposed, a single heavy-duty resistance heated furnace will be used. The fouled specimen tubes will be supported vertically in a taper sealed retort which is continuously flushed with fresh gases. A

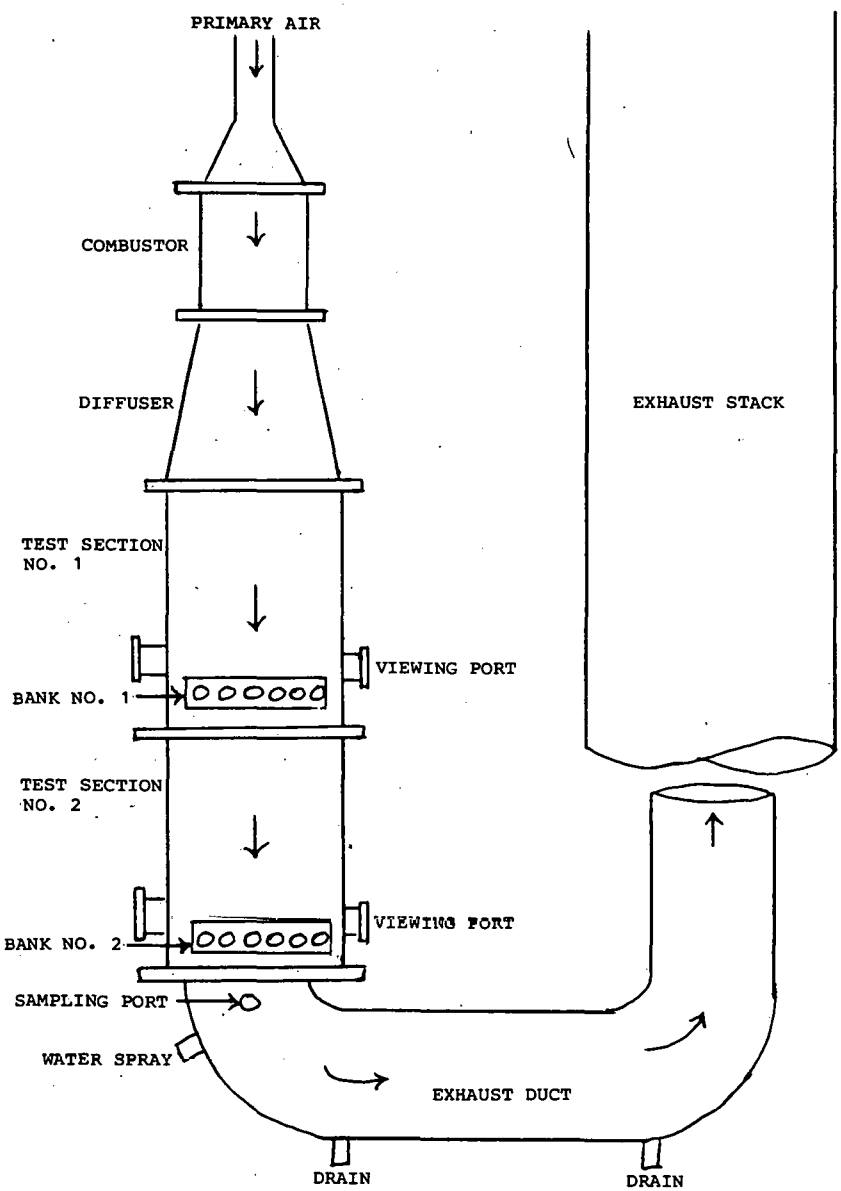

Figure 2. Schematic of Burner Rig Showing Major Components

specified mixture of three gases (simulating as closely as possible the gas environment in the combustor rig) will be mixed using several Sulzer static mixing elements which are composed of corrugated plates stacked to form open, intersecting channels to disrupt even relatively thin boundary layers between disproportional volumes of gases.

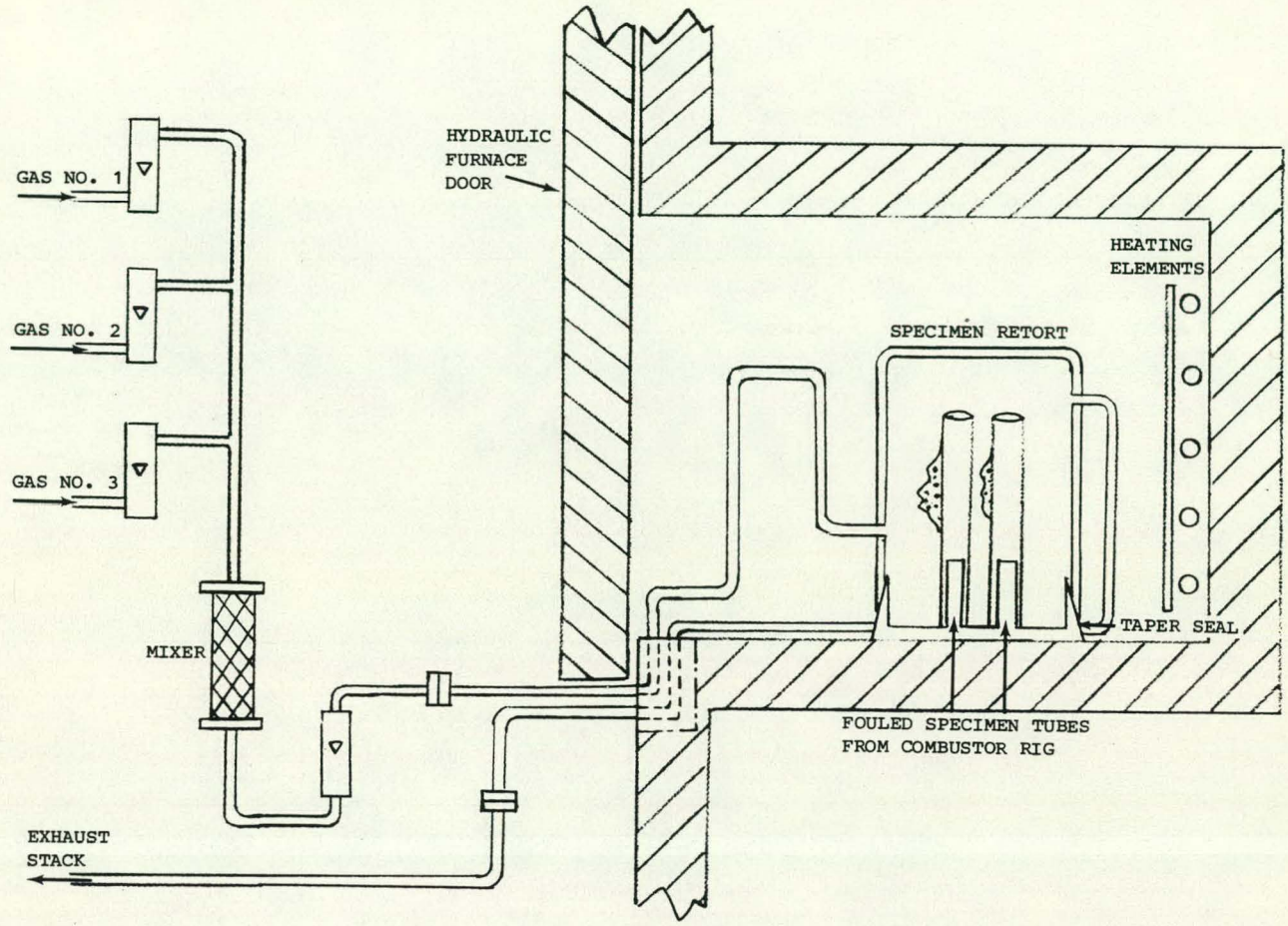

Figure 3. Schematic of Furnace Rig for Hot Corrosion Testing

3.2 TASK Ib - CONSTRUCTION OF TEST RIGS

Construction of the combustion test rig is approximately 80 percent complete. The next major step will be installation in the test cell. Figures 4 and 5 show photographs of the completed diffuser and test sections. The important features are labeled.

3.3 TASK Ic - CALIBRATION OF TEST RIGS

Preparatory to actual calibration of the combustion rig while operating, investigation into the required calibration techniques and operating parameters has been initiated. These include particle temperature measurement, calculations of particle temperature and velocity, and calculations to determine the required additives to produce the standard gas composition which is equivalent to a 0.2 percent sulfur coal. These items will be discussed separately.

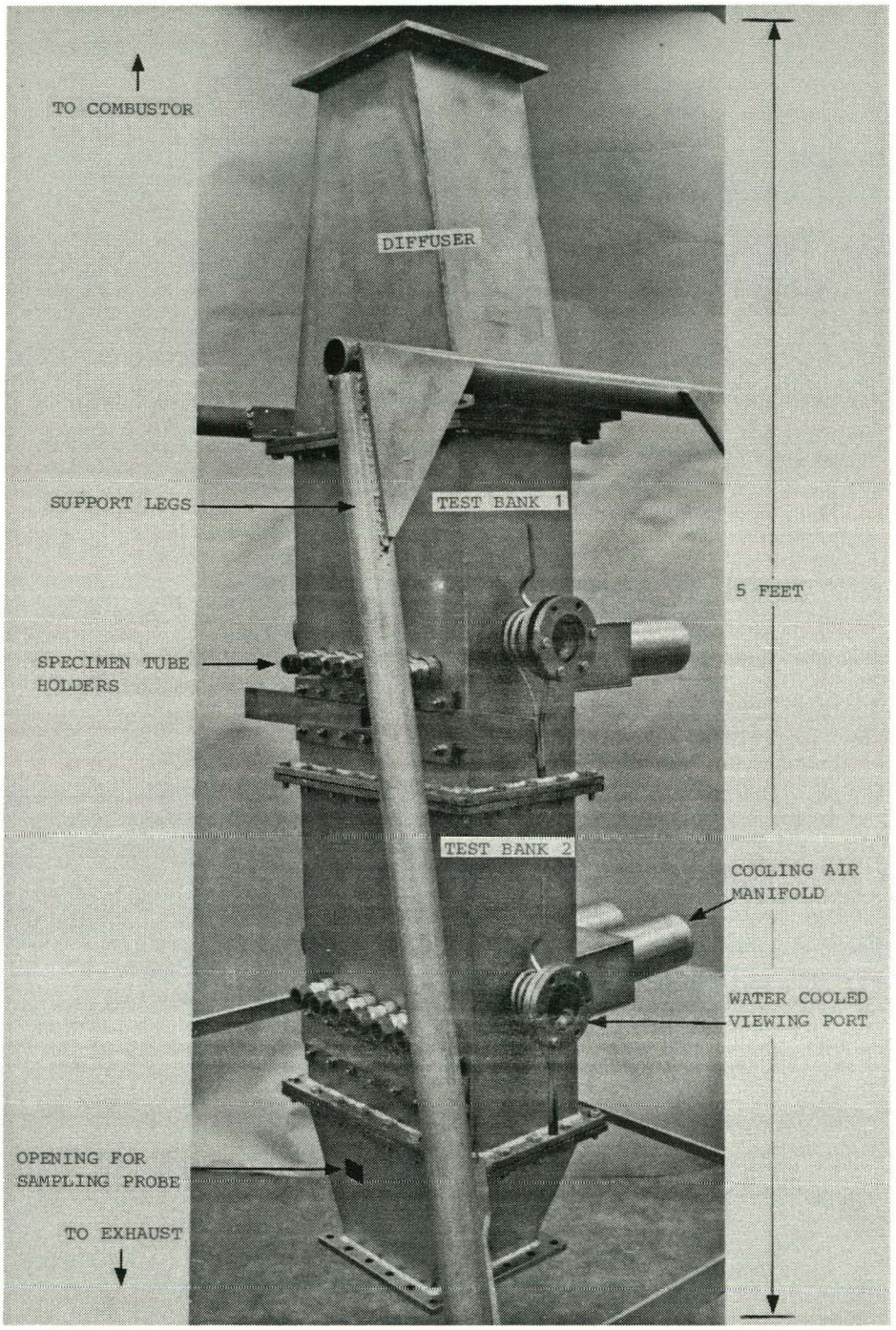

Figure 4. Combustion Rig - Diffuser and Test Sections

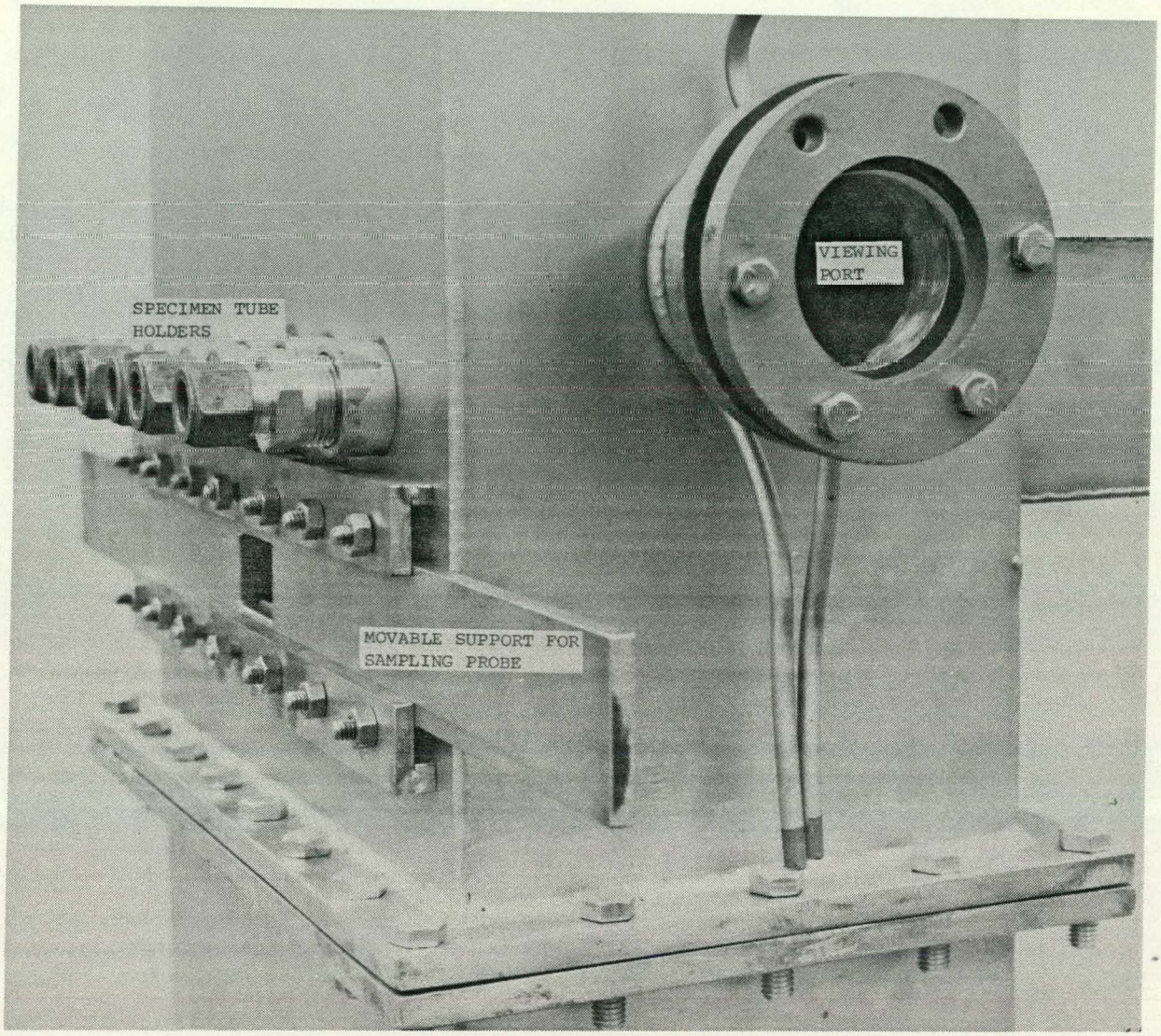

Figure 5. Outside View of Test Chamber

3.3.1 Particle Temperature Measurement

It is recognized that particle temperature and velocity measurements will be difficult to measure because of the small particle sizes (10 micron average) and the relatively low loading rates expected (1 lb/hr). Based on review of literature (Ref. 1) and available techniques, it was established that two color pyrometry (see App. B) would be a desirable method to measure particle temperature, primarily because of its reduced susceptibility to variations in target emissivities. Furthermore, it has been demonstrated (Ref. 2) that such dependence on emissivity is generally the largest source of error, and measurement errors using two-color pyrometry can be an order of magnitude less than optical pyrometry. On the other hand, the optical pyrometer is more sensitive and stable than the two color pyrometer. Besides consideration of the relative merits of the measurement techniques, it is anticipated

that the main difficulty will be trying to distinguish (i.e., focus upon) between the solid particles entrained in the hot gas stream and radiation from the gas itself and reflected radiation from the walls of the test section. In light of the anticipated scenario, the following strategies are proposed:

- Calibrate both two color and disappearing filament pyrometry using a perforated target (see Fig. 6) to simulate particles in the gas stream. Number of perforations will be based on the total number of particles within the field of view at any instant in time, given the expected loading rate.

- If two-color pyrometry is selected, the sensor head will be mounted at one of the viewing ports (water cooled to minimize heatup of the sensor unit) and the second viewing port directly across the test section will be replaced with a water cooled plate to reduce background radiative signals.

- If disappearing-filament pyrometry is selected, a piece of resistance heated metal strip (with a perforated plate) can be mounted at one viewing port to act as a comparator to the solid particles in the gas stream as monitored by a disappearing-filament pyrometer. Emissivity corrections will need to be rigorously applied.

3.3.2 Calculations of Particle Temperature and Velocity

Besides the empirical methods described above, particle temperature and velocity can be calculated, given certain assumptions. In the diffuser section, which forms a decelerating field, it is estimated that a minimum of 125 ft/sec gas velocity is required at the diffuser inlet to obtain the test velocity of 50 ft/sec at the diffusion outlet and subsquently through the test sections. Assuming that the particles are spherical and using the properties of pure Al_2O_3, equations of motion of 10 micron particles in the Stokesian regime ($R_e << 1.0$) can be formulated assuming that fluid drag is the only force acting in the direction of fluid and particle flow (see App. C for detailed treatment).

Similarly, by assuming that the spherical Al_2O_3 particles are moving in a gas stream of constant temperature, heat transfer equations can be set up and solved to determine rise in particle temperature along the diffuser section.

A computer code (App. C) was prepared to perform the differential calculations and selected results are given in Table 5 and plotted in Figures 7 and 8. From the data, it can be seen that even if the solid particles are at 70°F and zero ft/sec at the entrance to the diffuser, they will rapidly gain in temperature and velocity and will reach gas temperature in 5 milliseconds and gas velocity in 40 milliseconds. In terms of distance traveled, 6.4 and 30.4 inches are needed for the particles to reach gas temperature and velocity, respectively. Since the distance between the diffuser inlet and the first bank of specimens is 30 inches, it is anticipated that all particles in the gas stream will be at temperature and velocity prior to impingement on specimens. Calibration measurements will be performed to verify these calculated values.

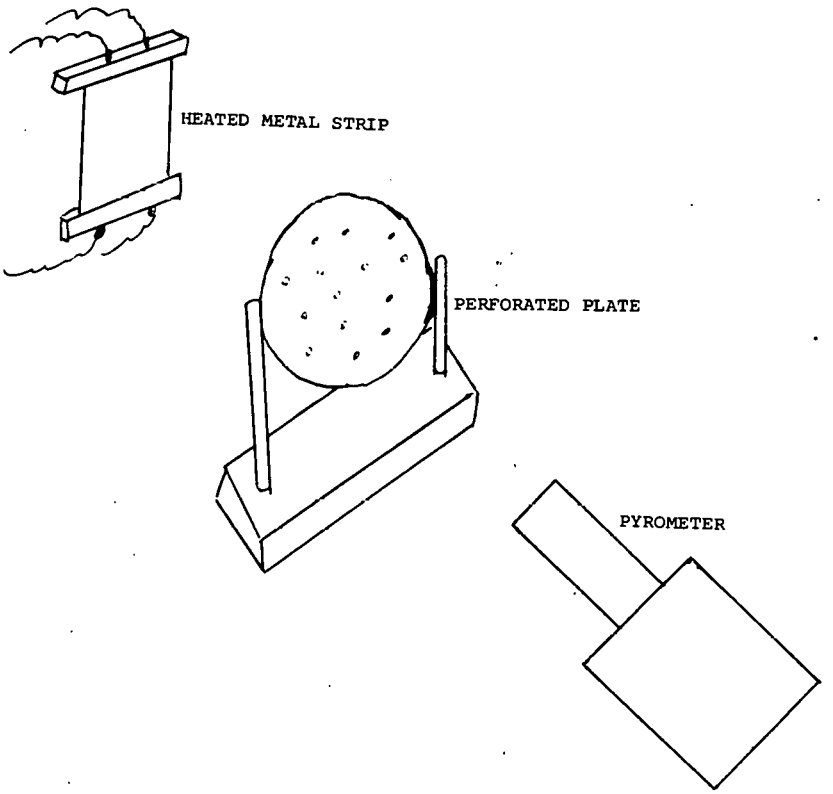

Figure 6. Calibration of Pyrometer Using Perforated Target Plate

Table 5

Changes in Particle Temperature, Particle Velocity and Gas Velocity With Increments in Time and Distance

Gas temperature - 2300°F (constant) Initial gas velocity = 125 ft/sec Initial particle temperature = 70°F Initial particle velocity = Zero ft/sec				
Time (sec)	Distance (inch)	Particle Temperature (°F)	Particle Velocity (ft/sec)	Gas Velocity (ft/sec)
0.00001	2.9×10^{-4}	149	5	125
0.00005	6.9×10^{-3}	434	22	125
0.0001	2.6×10^{-2}	734	41	125
0.0005	4.2×10^{-1}	1909	106	123
0.001	1.1	2235	119	120
0.005	6.4	2300	100	98
0.01	11.7	2300	77	76
0.04	30.4	2300	50	50

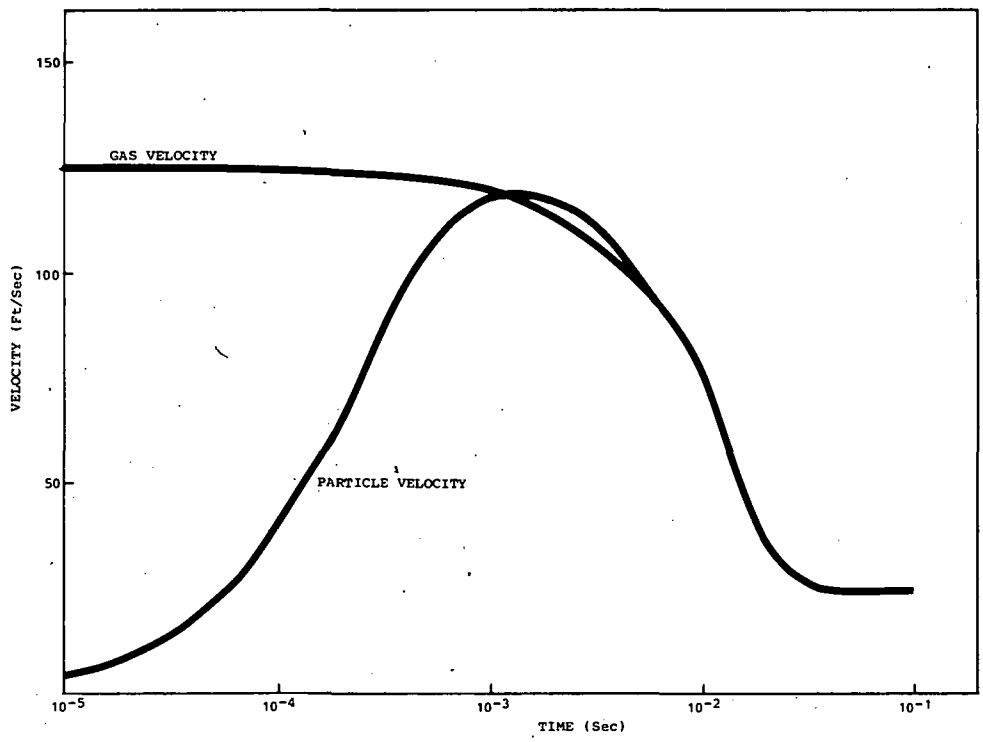

Figure 7. Particle Acceleration in Decelerating Gas Stream

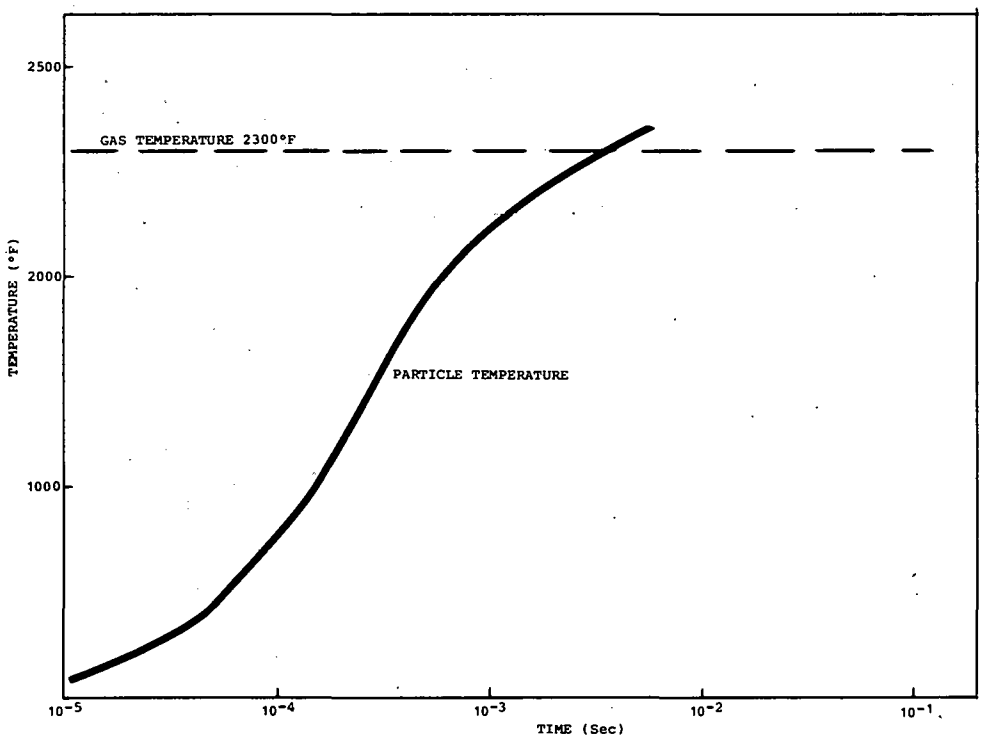

Figure 8. Particle Temperature Rise in Gas Stream of Constant Temperature

3.3.3 Derivation of "Standard" Combustion Environment

A typical analysis of San Diego natural gas is provided in Table 6. The sulfur content is generally in the order of parts per billion. For the purpose of this program, a "standard" natural gas containing a specified level of sulfur needs to be defined in order to form sulfur oxides in the gas phases. Since the partial pressures of the sulfur oxides in the test environment will also be affected by the equilibrium between the gases and the concentration of K_2SO_4, Na_2SO_4, etc., it is proposed that the sulfur level in natural gas will be determined equivalent to the flue gas composition of 0.2 percent sulfur coal. This sulfur level is probably the lower limit for a cleaned coal, but will provide enough sulfur oxides in the gas phase to minimize sulfate dissociation.

Table 6

Typical Analysis of San Diego Natural Gas

	Mole Percent
Propane	0.74
Isobutane	0.091
Natural Butane	0.146
Neopentane	0.019
Isopentane	0.144
Natural Pentane	0.137
Air	1.42
Methane	Balance
Carbon Dioxide	0.82
Pentanes and Higher	0.30
Propylene	0.03
Sulfur	ppb
Analysis done at Solar Turbines International May 28, 1981	

Calculations were performed to determine the amount of hydrogen sulfide gas to be added to natural gas. The calculations are based on San Diego natural gas and a high volatile lignite coal which is used in Solar's pulverized coal combustor. The coal analysis is shown in Table 7. Typically, this coal contains 0.5 weight percent sulfur, and in the calculations this was reduced to 0.2 weight percent with the balance added to carbon. Details of the procedure used are given in Appendix D.

Results show that the volume ratio of H_2S to natural gas is 0.002.

Table 7

Analysis of High Volatile Lignite Coal
Used at Solar Turbines International

Lab No. 46775			
Proximate	As Rec'd	Air Dry	Oven Dry
Moisture (%)	6.37	6.37	0.00
Ash (%)	7.05	7.05	7.53
Volatile (%)	35.45	35.45	37.87
Fixed Carbon (%)	51.13	51.13	54.60
Total	100.00	100.00	100.00
Sulfur (%)	0.52	0.52	0.56
BTU, per pound	11970	11970	12785
BTU, per pound, Ash, Moisture-Free			13827
Ultimate			
Carbon (%)	68.07 (68.39)*	68.07	72.71
Hydrogen (%)	5.53	5.54	5.14
Nitrogen (%)	1.35	1.35	1.44
Oxygen (%)	17.48	17.48	12.62
Ash (%)	7.05	7.05	7.53
Sulfur (%)	0.52 (0.2)*	0.52	0.56
Total	100.00	100.00	100.00

* Values used in calculations for H_2S concentration.

Analyses performed at Northern Testing Laboratory
Coal from Colorado Westmorland Coal Company

4

FUTURE WORK

During the next reporting period the combustion test rig will be installed in the test cell and calibration will be initiated. The furnace rig will be constructed.

THIS PAGE

WAS INTENTIONALLY

LEFT BLANK

REFERENCES

1. Ayling, A.B. and Smith, I.W., "Measurement Temperatures of Burning Pulverized Fuel Particles and the Nature of the Primary Reaction Product", Combustion and Flame, V. 18, p. 173 (1972).

2. Technical Publication of Milletron, Inc., "Radiation Pyrometry".

THIS PAGE

WAS INTENTIONALLY

LEFT BLANK

APPENDIX A

THE COMBUSTOR RIG

THIS PAGE

WAS INTENTIONALLY

LEFT BLANK

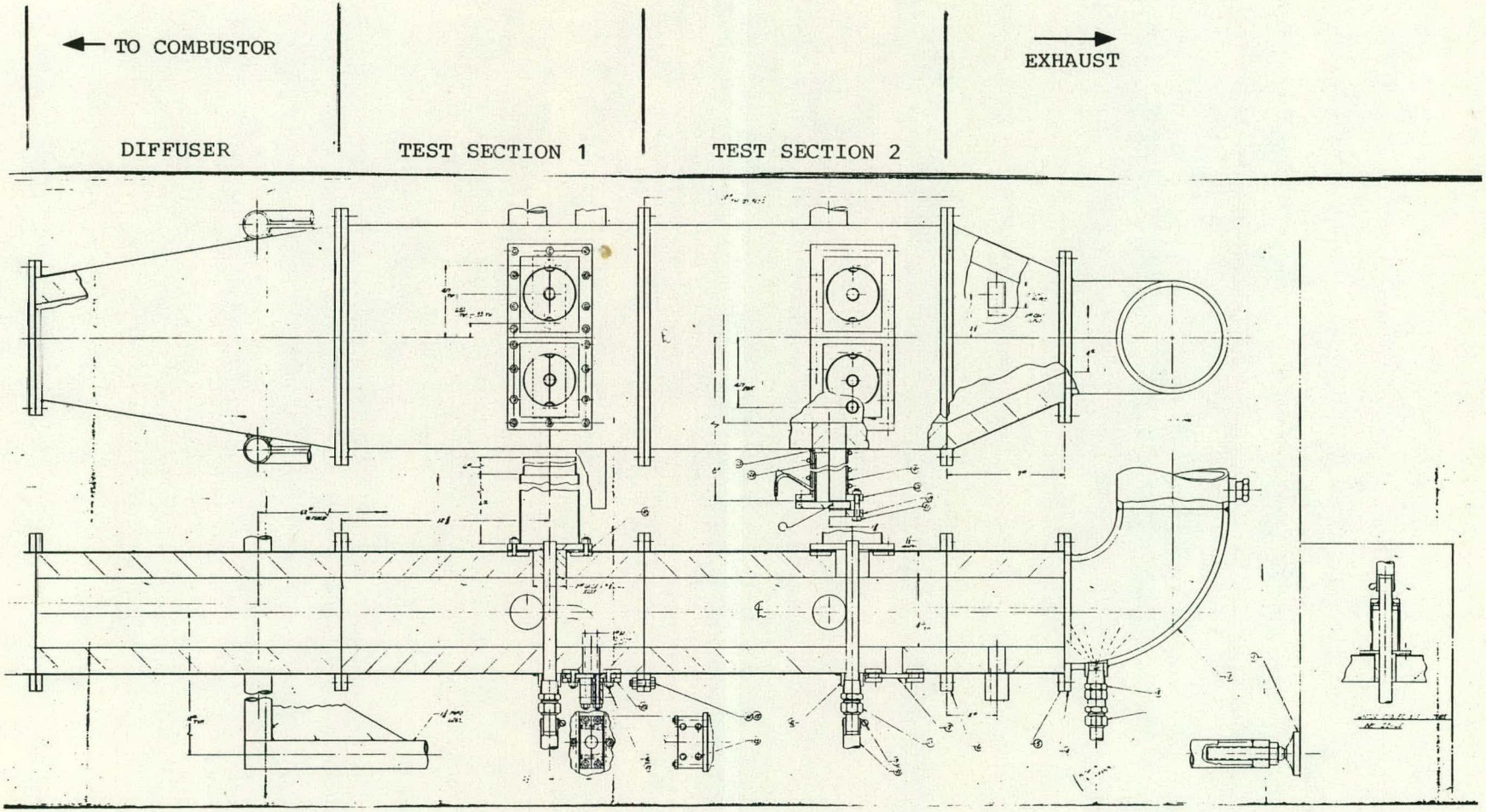

Figure A-1. Combustion Rig - Drawing of Diffuser and Test Sections
(To scale, reduced 95 percent)

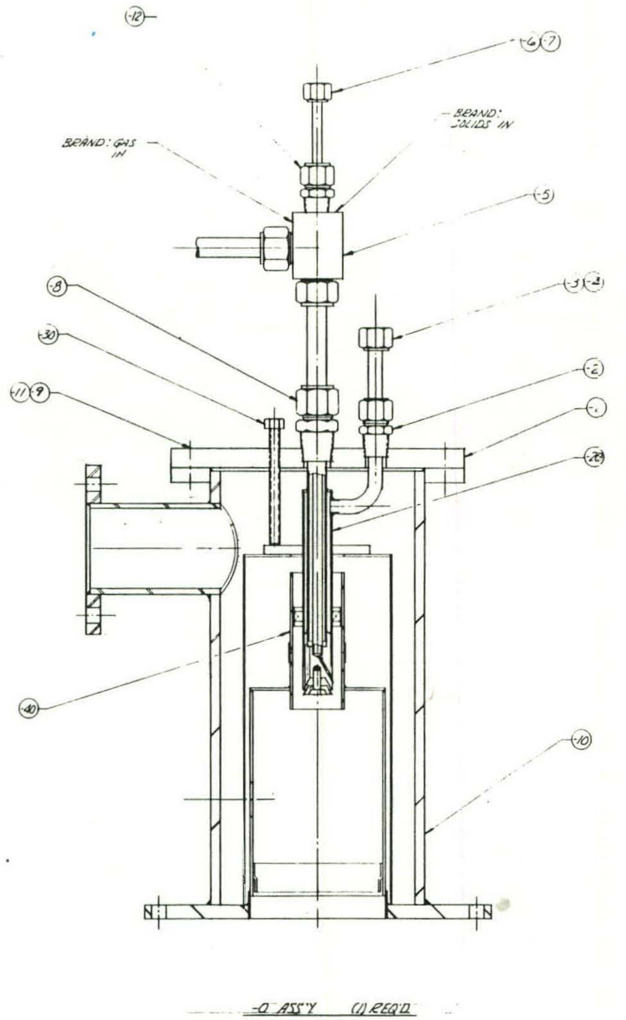

-40	-30	-20	-10	-0	Part Number	Description	Material	Specification	Unit Wt
				1	-40	SLEEVE	ASS'Y.		
			1		-38	BOSS	.375X1.25 [illegible]	304 ST. STL.	
			4		-37	BOSS	.75 DIA. [illegible]	304 ST. STL.	
			1		-36	BOSS	.75 DIA BAR	304 ST. STL.	
		1			-35	PLATE	.25 PLATE	CARBON STL.	
		1			-34	COLLAR	.06 SHT.	304 ST. STL.	
	1				-33	HEX. NUT	.25-20	316 ST. STL.	
	1				-32	THD. ROD	.25-20	316 ST. STL.	
1					-31	RING	.06 SHT.	304 ST. STL.	
				3	-30	JACK ASS'Y			
1					-29	COLLAR	.06 SHT	304 ST. STL.	
			1		-28	FLANGE	.375 PLATE	CARBON STL.	
			1		-27	PIPE	2" SCHED 40	CARBON STL.	
			1		-26	FLANGE	.375 PLATE	CARBON STL.	
			1		-25	PIPE	5.0" SCHED 40	CARBON STL.	
			1		-24	RING	.06 SHT.	HAST. "X"	
			1		-23	FLANGE	.375 PLT.	1020 CRS.	
		14			-22	BLADE	.02 SHT.	304 ST. STL.	
		1			-21	TUBE	.375%X.035 [illegible]	304 ST. STL.	
				1	-20	NOZZLE	ASS'Y.		
		1			-19	TUBE	.25%X.035 [illegible]	304 ST. STL.	
		1			-18	TUBE	.50%X.035 [illegible]	304 ST. STL.	
		1			-17	CAP	.06 SHT	304 ST. STL.	
		1			-16	TUBE	.75%X.035 [illegible]	304 ST. STL.	
		1			-15	NOZZLE	1" DIA BAR	304 ST. STL.	
		1			-14	CUP	1" DIA BAR	304 ST. STL.	
		1			-13	PIN	.187 DIA RD.	304 ST. STL.	
				1	-12	MALE CONNECTOR	4-6 FBZ-SS	PARKER C.P.I.	
				26	-11	HEX. NUT	.375-16	316 ST. STL.	
				1	-10	HOUSING ASS'Y			
				26	-9	HEX HD BOLT	.375-16X1.25	316 ST. STL.	
				1	-8	[illegible] CONNECTOR	8-8FMBZ-SS	PARKER C.P.I.	
				1	-7	TUBE FERRULE	4-TZ-SS	PARKER C.P.I.	
				1	-6	TUBE NUT	4-BZ-SS	PARKER C.P.I.	
				1	-5	FEMALE RUN TEE	8-6-8-MBZ-SS	PARKER C.P.I.	
				1	-4	TUBE FERRULE	6-TZ-SS	PARKER C.P.I.	
				1	-3	TUBE NUT	6-BZ-SS	PARKER C.P.I.	
				1	-2	[illegible] CONNECTOR	6-6 FMBZ-SS	PARKER C.P.I.	
				1	-1	PLATE	.50 PLATE	1020 CARBON STL.	

QTY REQD — ← ASSY NO. — LIST OF MATERIAL (PARTS LIST)

SOLAR TURBINES INTERNATIONAL

APPROVED BY / GOVT CONTRACT NO.	DRAWING TITLE: INJECTOR- FUEL LIQUIDS & SOLIDS
RITZ 6-3-81	
RITZ 6-3-81	
DESIGN ACTIVITY: RESEARCH	SIZE: E — CODE IDENT NO.: 55820 — DRAWING NO.: RSK 2301004
CUSTOMER: D.O.E./P.E.T.C.	SCALE: FULL — SHEET 1 OF 3

Figure A-2. Combustion Rig - Combustor and Injector (Sheet 1 of 3)

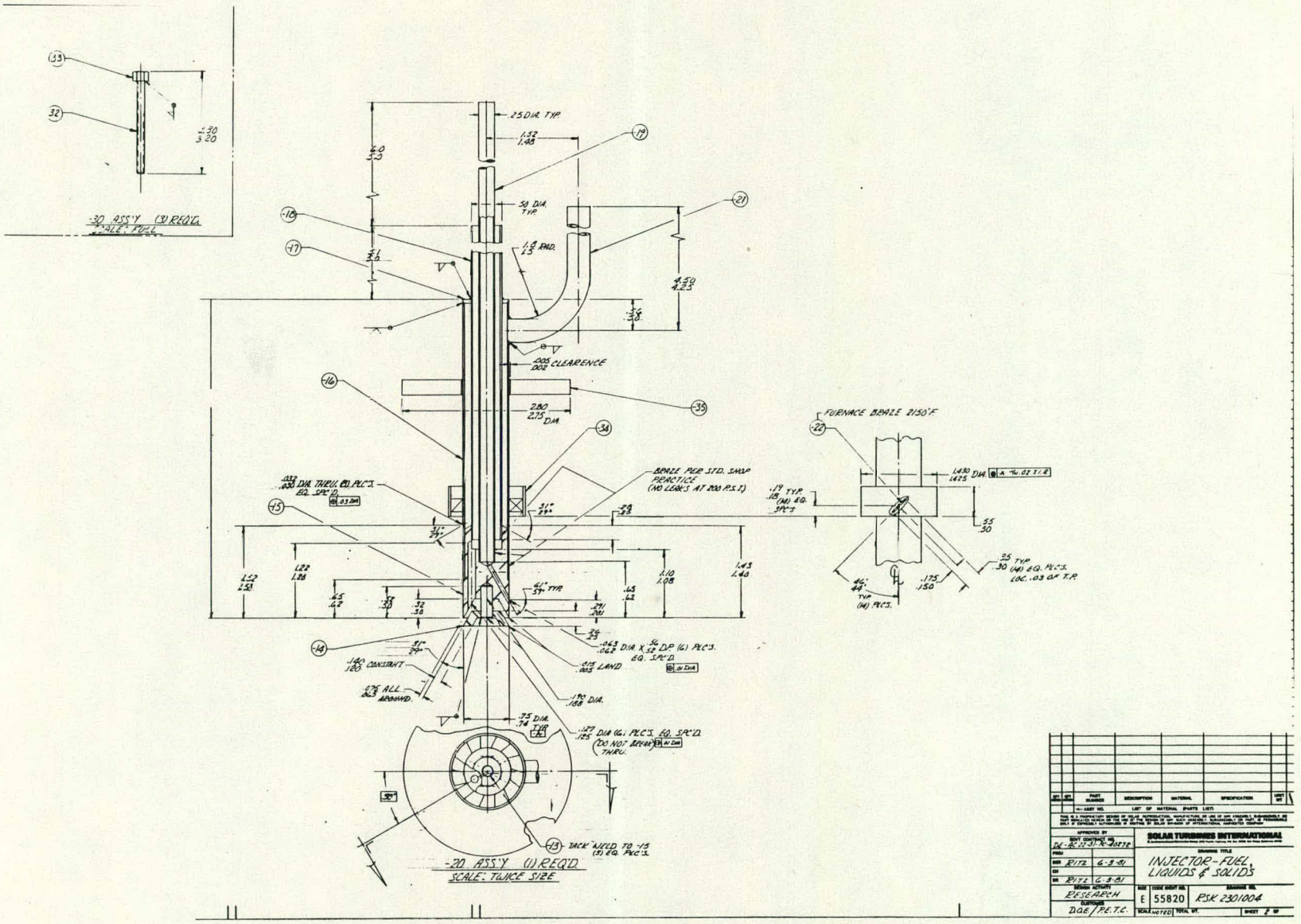

Figure A-2. Combustion Rig - Combustor and Injector (Sheet 2 of 3)

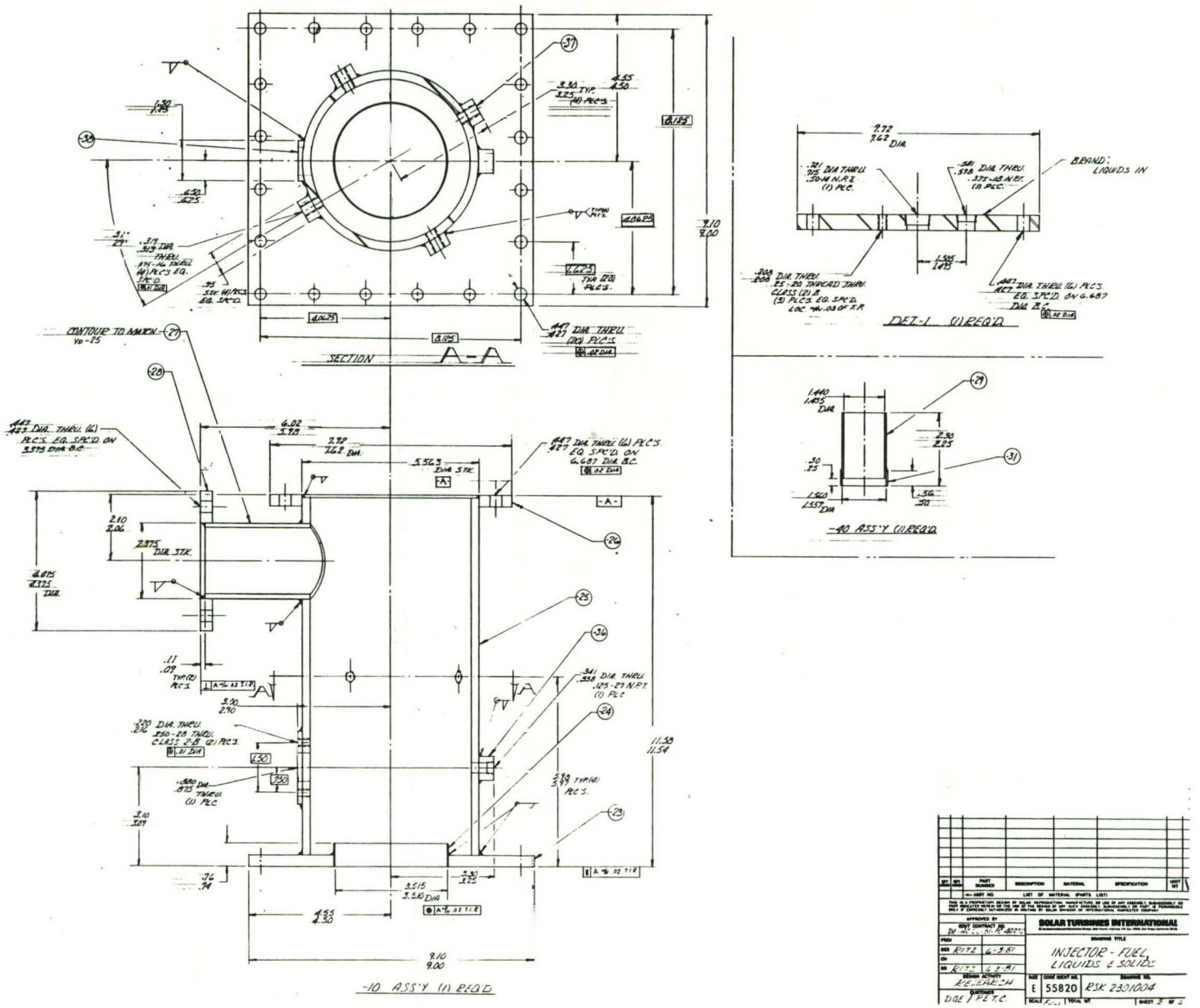

Figure A-2. Combustion Rig - Combustor and Injector (Sheet 3 of 3)

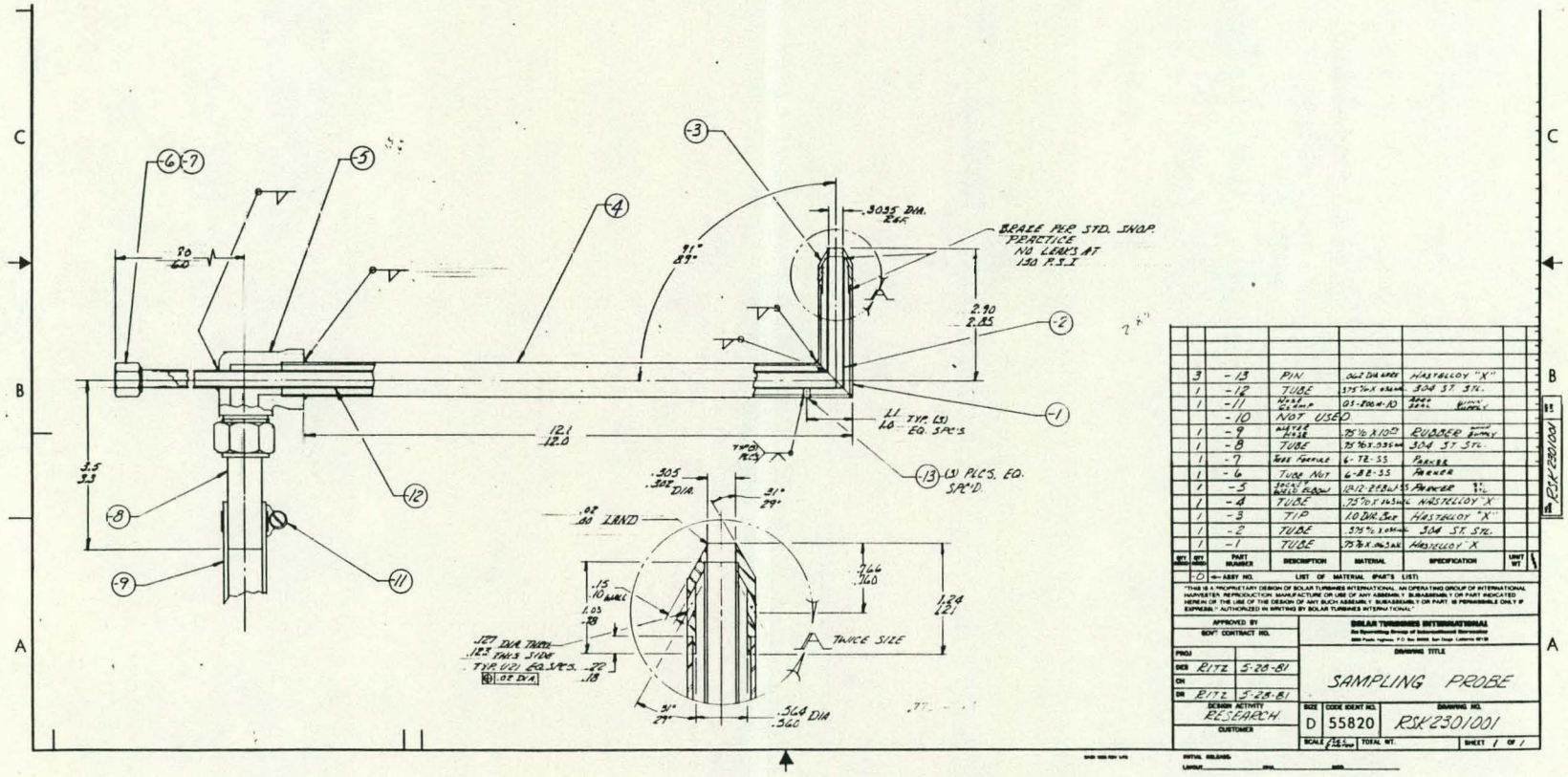

Figure A-3. Sampling Probe (Sheet 1 of 2)

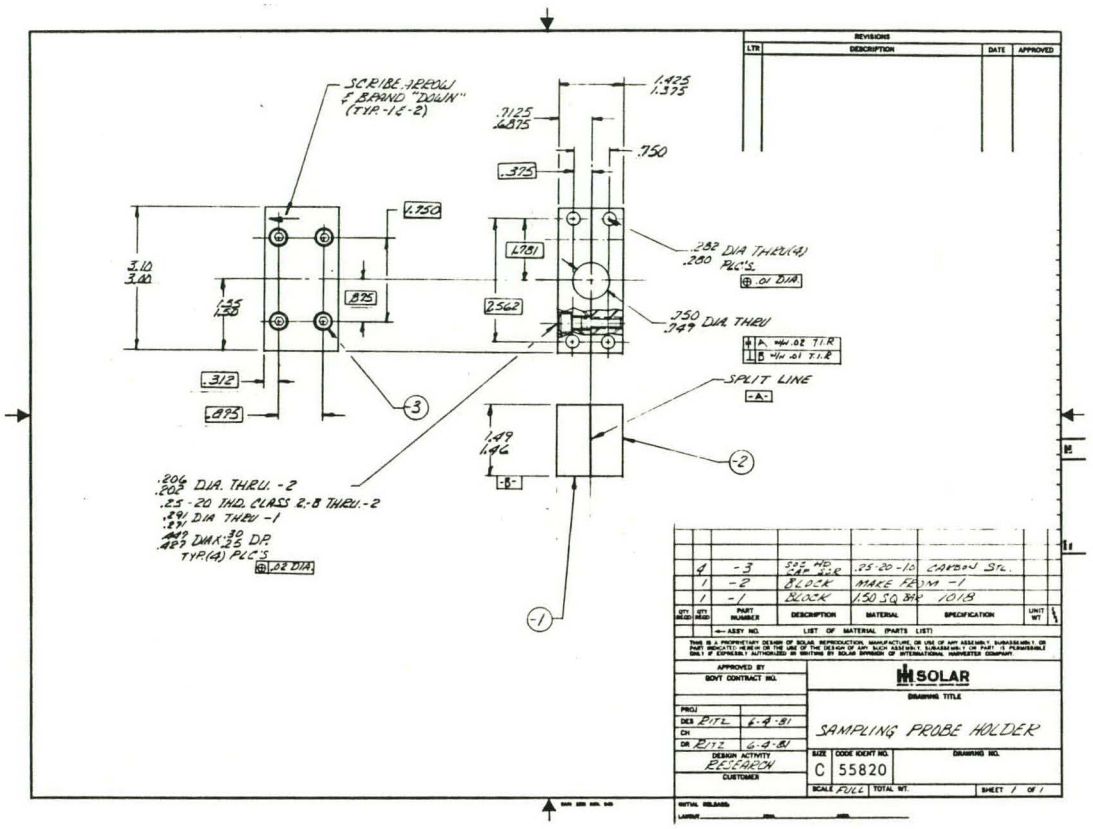

Figure A-3. Sampling Probe (Sheet 2 of 2)

APPENDIX B

TWO-COLOR PYROMETER

THIS PAGE

WAS INTENTIONALLY

LEFT BLANK

APPENDIX B

TWO-COLOR PYROMETRY

The ratio pyrometer in a sense starts off by consisting of two brightness pyrometers. The energy around one fixed wavelength is measured as is the energy around a second fixed wavelength which is located close to the first wavelength. The energy obtained from the first measurement is then divided by the energy obtained from the second one and a ratio of these energies is obtained. This ratio is a measurement of the temperature.

Mathematically, the properties of the instrument can be seen from Wien's Law. If we write Wien's Law giving the energy at each of the two selected wavelengths, we have for the first wavelength

$$H(\lambda_1 T) = \varepsilon_{\lambda_1} c_1 \lambda_1^{-5} e^{-c_2/\lambda_1 T}$$

and for the second wavelength

$$H(\lambda_2 T) = \varepsilon_{\lambda_2} c_1 \lambda_2^{-5} e^{-c_2/\lambda_2 T}$$

If we now take the ratio of the two energies

$$\text{Ratio} = \frac{\varepsilon_{\lambda_1}}{\varepsilon_{\lambda_2}} \frac{\lambda_1^{-5} e^{-c_2/\lambda_1 T}}{\lambda_2^{-5} e^{-c_2/\lambda_2 T}}$$

We can now see that the ratio is not a direct function of the emissivity, but rather is a function of the ratio of emissivities $\epsilon_{\lambda 1}/\epsilon_{\lambda 2}$ and of course the temperature. If the two wavelengths are chosen closely enough together, the ratio of the emissivities becomes 1 and the measurement does not depend on emissivity. This is the "gray" body condition where the emissivities are identical for the wavelengths of interest. It will be noted for the gray body that the emissivity ratio will drop out of the equation whether the actual values of emissivity are 0.9 or 0.1. Hence, low absolute emissivity value materials which create the largest errors for the brightness and total radiation pyrometers do not bother the ratio pyrometer. The only question is how much does the spectral emissivity vary from one selected wavelength to another.

The selection of the two wavelengths usually has to be made on the basis of obtaining sufficient sensitivity for a measurement. Obviously, if the two wavelengths selected were the same or extremely close to each other, the energy ratio obtained would always be 1 and no temperature information could be derived. Fortunately, the wavelengths can be located for good sensitivity and high freedom from emissivity effects.

If the ratio of spectral emissivities $\epsilon_{\lambda_1}/\epsilon_{\lambda_2}$ is not constant, however, the two-color pyrometer can exhibit a small measurement error. This error can be derived in the form of the brightness pyrometer error to be

$$T_T = \frac{T_R}{1 + \frac{\lambda_2 \lambda_1}{\lambda_2 - \lambda_1} \frac{T_R}{C_2} \ln \frac{\epsilon_{\lambda_1}}{\epsilon_{\lambda_2}}}$$

where T_T is again the true temperature and T_R is the ratio temperature or the reading of the ratio pyrometer.

From this equation, direct dependence on the logarithm of spectral emissivity has been replaced by a dependence on the logarithm of the emissivity ratio. It will be noted that if ϵ_{λ_1} is smaller than ϵ_{λ_2}, the logarithm term will be negative and again the ratio temperature reading will be less than the true reading. On the other hand, if ϵ_{λ_1} is larger than ϵ_{λ_2}, the ratio temperature reading can be above the true temperature reading.

APPENDIX C

DYNAMICS OF PARTICULATE CLOUDS

THIS PAGE

WAS INTENTIONALLY

LEFT BLANK

APPENDIX C

DYNAMICS OF PARTICULATE CLOUDS

Equation of Motion - A particle moving through a fluid with instantaneous velocity $\vec{V}$ will experience a resisting force given by

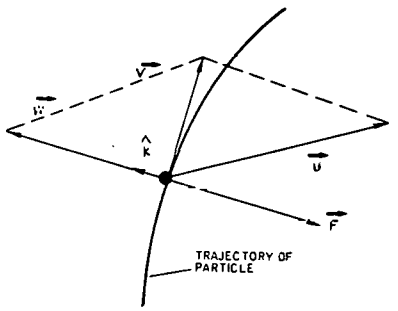

$$\vec{F} = -\frac{1}{2}\rho(\vec{V}-\vec{U})^2 C_D A\hat{K}$$

$$= -\frac{1}{2}\rho(\vec{W})^2 C_D A\hat{K}$$

where $\vec{U}$ = local velocity of the fluid

$\vec{W}$ = velocity of the particle relative to fluid = $\vec{V} - \vec{U}$

ρ = density of the fluid

C_D = drag coefficient of the particle

A = relevant projected area of the particle for the given drag coefficient

$\hat{K}$ = unit vector in the direction or relative motion

Neglecting all other body forces (including gravity), the equation of motion of the particle will be

$$m\frac{d\vec{V}}{dt} = \vec{F} = -\frac{1}{2}\rho(\vec{W})^2 C_D A\hat{K}$$

where m = mass of the particle

or $$\frac{d}{dt}(\vec{U}+\vec{W}) = -\frac{C_D A\rho}{2m}(\vec{W})^2\hat{K}$$

Particle Velocity Calculation

If the particle is spherical of diameter D_p and density ρ_p, then

$$m = \rho_p \, D_p^3/6 \, \pi$$

and a good approximation to the drag coefficient is

$$C_D = 0.4 + 24/Re$$

with $A = \pi D^2/4$ the projected frontal area

Also, $$Re = |\vec{W}| \, D_p \rho/\mu$$

where μ = absolute viscosity of the fluid

If additionally, $\vec{V}$ is in the same direction as $\vec{U}$, then $-\vec{W}$ is also in this same direction, and with $\vec{U} = -UK$, $\vec{V} = -VK$, and $\vec{W} = WK$, we get the scalar equations

$$W = U - V$$

and $$\frac{d}{dt}(-U + W) = -\frac{1}{2} \frac{6}{\rho_p D_p^2} (0.4 + 24\mu/WD_p) \, \pi D^2/4 \, W^2$$

$$= \frac{0.3}{\rho_p D_p} W^2 + 18\mu/\rho_p D_p^2 \, W$$

The factor $18\mu/\rho_p D_p^2 = a/\tau$ where τ is the Stokesian time constant associated with the range when U = 0. Also, if U is a constant velocity (i.e., a uniform fluid velocity field),

$$d/dt \, (-U + W) = dW/dt$$

Putting $0.3\rho/\rho_p D_p = 1/\delta$, we get

$$dW/dt = -1/\tau \, (W + \tau/\delta \, W^2)$$

By defining time increments, Δt, the above equations can be iteratively calculated to obtain particle velocity and travel.

Particle Temperature Calculation

Assuming a spherical particle moving in a gas stream of constant temperature, a Reynold's number can be calculated for each increment of length along the duct, based on a relative mean velocity between the particle and the gas stream. The heat transfer equations used are as follows:

$$- C_{p_1} \rho dT = h A_s (T - T_\infty) d\theta$$

Change in internal energy of particle during time interval $d\theta$

Net heat flow from gas to particle during $d\theta$

where,

C_{p_1} = specific heat of particle Btu/lb°F

ρ = density of particle lb/ft^3

h = heat transfer coefficient - Btu/lb-hr

dT = temperature change during $d\theta$ = °F

A_s = surface area of particle ft^2

$d\theta$ = time internal - hr

T = average temperture of particle °F

T_∞ = free stream temperature °F

Separating variables and integrating

$$(T - T_\infty) / (T_o - T_\infty) = \exp -(h A_s / C_p \rho V) \theta$$

where

T_o = initial particle temperature °F

T_∞ = final particle temperature °F

V = particle volume - ft^3

If the Reynold's number $1.0 < Re < 25$.

$$h = C_{p_2} V_{rel} \rho_\infty \left(2.2/Re_D + 0.48/Re_D^{0.5}\right)$$

where

$$Re_D = V_{rel} \rho_\infty D_o/\mu f$$

C_{p_2} = specific heat of gas

V_{rel} = air stream and particle relative velocity

ρ_∞ = gas density

μf = gas viscosity

APPENDIX D

CALCULATIONS TO DETERMINE AMOUNT OF H_2S TO BE ADDED TO NATURAL GAS TO PROVIDE STANDARD TEST ENVIRONMENT

THIS PAGE

WAS INTENTIONALLY

LEFT BLANK

APPENDIX D

CALCULATIONS TO DETERMINE AMOUNT OF H_2S TO BE ADDED TO NATURAL GAS TO PROVIDE STANDARD TEST ENVIRONMENT

Using the analysis for San Diego natural gas and Colorado Westmorland coal provided in Tables 6 and 7, heat balance calculations were performed using established computer programs. The basis of each set of calculations was the 2300°F combustion product temperature. With each fuel, complete combustion was assumed and with the known heating value, the fuel-to-air ratio can be determined that is needed to produce 2300°F combustion gas temperature.

The procedure for calculation of natural gas combustion is standard and routinely employed in the gas turbine industry.

The solid fuel calculations were performed using mass and energy balance for a coal combustor at a given excess air fraction, fuel composition, ambient humidity, fuel heat value, and degree of incomplete combustion for oxidizing or stoichiometric conditions. Chemical equilibrium effects are <u>not</u> considered for the flue gas constituents or the solids. All reactions are considered to be complete, with the exception of the carbon and sulfur reactions on which restraints are placed by the input. The following reactions are considered:

$$C + O_2 \quad -- \quad CO_2$$
$$C + 1/2\ O_2 \quad -- \quad CO$$
$$S + 1/2\ O_2 \quad -- \quad SO_2$$
$$2H + 1/2\ O_2 \quad -- \quad H_2O$$
$$H + Cl \quad -- \quad HCl$$

The reduction in full heat value due to unburned carbon is calculated assuming products of combustion:

1. The temperature rise of the products of desired combustion are calculated given the flue gas temperature.

2. The flue gas temperature is calculated given a desired combustion temperature.

If option one is performed the subroutine performs a half interval search to determine the flue gas temperature. Iteration is required because the flue gas properties are a function of temperature. The solid products of combustion are assigned a mean specific heat vale of 25 BTU/lbm°F for the temperature rise calculations.

LIMITATIONS/ASSUMPTIONS

1. The subroutine assumes latent heat of vaporization of water is 1050 BTU/LBM. Water content of fuel is assumed to enter combustor as saturated liquid at atmospheric pressure.

2. Gas properties used are limited between 70 and 4500°F. The gas properties should be expanded to allow calculations for -20°F days.

3. Capacity to calculate excess air required for a given combustor temperature and in-bed heat exchanger duty are not yet present. This can be accomplished by iterating once using the option for dilution with ambient air.

4. The in-bed heat exchanger duty is expressed as BTU/LB fuel. This is an inconvenient unit to work with unless an adiabatic combustor is desired. The heat exchanger performance could be expressed more conveniently by specifying a mass flow and effectiveness or an effectiveness and a fraction of available heat extracted.

5. No prediction of solids carry-over into the flue gas stream is predicted.

6. A second law analysis of the combustion process is not included. Second law analysis would necessitate the specification or calculation of pressure drops through system.

7. An option to allow the subroutine to calculate the higher heat value of the fuel from its composition may be added.

The results show that with 0.002 moles H_2S/moles of natural gas, the SO_2 concentration in 2300°F adiabatic flame would be equivalent to that burning 0.2 weight percent coal such as is shown below:

	H_2S Doped Natural Gas	0.2 w/o Sulfur Coal
N_2	73.11	74.24
CO_2	5.16	8.67
O_2	9.68	10.01
H_2O	11.17	6.13
SO_2	0.0094	0.0095